

# Periodic self-lensing from accreting massive black hole binaries

Daniel J. D’Orazio<sup>★</sup> and Rosanne Di Stefano

*Astronomy Department, Harvard University, 60 Garden Street, Cambridge, MA 02138, USA*

Accepted 2017 October 30. Received 2017 October 24; in original form 2017 July 10

## ABSTRACT

Nearly 150 massive black hole binary (MBHB) candidates at sub-pc orbital separations have been reported in recent literature. Nevertheless, the definitive detection of even a single such object remains elusive. If at least one of the black holes is accreting, the light emitted from its accretion disc will be lensed by the other black hole for binary orbital inclinations near to the line of sight. This binary self-lensing could provide a unique signature of compact MBHB systems. We show that, for MBHBs with masses in the range  $10^6$ – $10^{10} M_{\odot}$  and with orbital periods less than  $\sim 10$  yr, strong lensing events should occur in one to 10s of per cent of MBHB systems that are monitored for an entire orbit. Lensing events will last from days for the less massive, shorter period MBHBs to a year for the most massive  $\sim 10$  year orbital period MBHBs. At small inclinations of the binary orbit to the line of sight, lensing must occur and will be accompanied by periodicity due to the relativistic Doppler boost. Flares at the same phase as the otherwise average flux of the Doppler modulation would be a smoking gun signature of self-lensing and can be used to constrain binary parameters. For MBHBs with separation  $\gtrsim 100$  Schwarzschild radii, we show that finite-sized source effects could serve as a probe of MBH accretion disc structure. Finally, we stress that our lensing probability estimate implies that  $\sim 10$  of the known MBHB candidates identified through quasar periodicity should exhibit strong lensing flares.

**Key words:** accretion, accretion discs – gravitational lensing: micro – quasars: supermassive black holes.

## 1 INTRODUCTION

The merger of two galaxies, each containing a massive black hole (MBH), can yield a compact, massive black hole binary (MBHB; Kormendy & Richstone 1995; Kauffmann & Haehnelt 2000; Ferrarese & Ford 2005; Kormendy & Ho 2013). The MBHBs may merge, producing gravitational radiation (Begelman, Blandford & Rees 1980). Discoveries of MBHBs therefore allow us to learn about past galaxy interactions and to predict important future events. Such systems can be identified electromagnetically only if matter falling on to the MBH(s) emits light. In recent years, active galactic nuclei (AGN) have been examined for evidence that the accreting MBH that powers it may be in a binary. Most relevant to this study, recent time-domain surveys have selected MBHB candidates by identifying periodically varying optical emission from such an AGN (Graham et al. 2015a,b; Charisi et al. 2016). The periodicity could be caused by variable accretion on to a binary (Hayasaki, Mineshige & Sudou 2007; MacFadyen & Milosavljević 2008; Cuadra et al. 2009; Noble et al. 2012; Roedig et al. 2012; Shi et al. 2012; D’Orazio, Haiman & MacFadyen 2013; Farris et al. 2014, 2015; Gold et al. 2014a,b; Dunhill, Cuadra & Dougados 2015; Shi & Krolik 2015; D’Orazio et al. 2015a, 2016; Muñoz

& Lai 2016), or relativistic Doppler boost of emission emanating from gas bound to the orbiting BHs (D’Orazio, Haiman & Schiminovich 2015b).

In this paper we explore a signature which can help to discover more MBHB candidates, vet the candidacy of systems identified in other ways, measure the binary’s orbital parameters, and help to map the accretion geometry. Specifically, we consider the gravitational lensing of the accretion flow of one BH by its companion. Binary self-lensing is a phenomenon that must occur in systems with favourable orientations (see also Rahvar, Mehrabi & Dominik 2011). We will show that self-lensing is expected in a non-negligible number (a few to 10s of per cent depending on binary parameters) of accreting MBHBs.

We compute the lensing effects and show that they can be detected and correctly interpreted. The signatures of self-lensing are most dramatic if the MBHB has mass near or above  $10^6 M_{\odot}$  and a small orbital inclination to the line of sight. Lensing produces a flare at specific values of the orbital phase. The duration of this flare is proportional to the square root of the mass of the lensing BH and can range from days to years for MBHBs depending on the binary orbital period, mass, and mass ratio.

Small binary orbital inclinations also favour detection of periodicity generated by the relativistic Doppler boost. If the accretion disc emission is observed to be modulated in time due to the relativistic Doppler effect, then the lensing signatures must occur at a

<sup>★</sup> E-mail: [daniel.dorazio@cfa.harvard.edu](mailto:daniel.dorazio@cfa.harvard.edu)

specific phase in the Doppler-boost light curve, namely at the times of average brightness when one BH is behind the other, moving transverse to the line of sight. Hence, for example, an observation of lensing flares at what would otherwise be the flux averages of a nearly sinusoidal light curve would provide strong evidence for a MBHB and for the Doppler-boost interpretation.

We show that, depending on the binary separation and masses of the BHs, the accretion disc source can act either as a point source or a finite-sized source. In the point-source case, a unique identifier of the lensing event is its appearance in all wavelengths, because gravitational lensing is achromatic. We discuss in Section 3, however, the practical difficulties that may be associated with determining achromaticity in a real MBHB system. Assuming that the disc size is proportional to the Hill radius, finite-sized source lensing will become important for larger separation binaries and cause wavelength-dependent lensing flares. Wavelength dependence arises because the accretion disc will emit at different wavelengths at different radii; hence, a lensing event of an accretion disc in the finite-sized source case will probe the accretion flow around the lensed BHs. In cases where there are two discs, one for each BH, the achromaticity of lensing will allow us to distinguish the spectra of the individual discs and possibly the circumbinary disc.

Finally, once the existence of a specific MBHB for which we observe gravitational lensing is firmly established, any future changes in the emission from the BH can be studied in more detail than would otherwise be possible through the magnification effects of the ‘telescopes’ provided by the BHs themselves.

## 2 LENSING CALCULATIONS

## 2.1 System scales

We envision the galactic merger process delivering MBHs and gas to the centre of a newly formed galaxy (Barnes & Hernquist 1992; Barnes & Hernquist 1996; Barnes 2002; Mayer 2013). When the MBHBs harden sufficiently (sub-pc separations), they can be surrounded by a circumbinary gaseous disc. This disc feeds ‘mini-discs’, which are bound to, and feed each individual MBH. Such gas accretion can generate bright emission, as in the case of a single MBH, but modulated at the binary orbital period and its multiples (e.g. D’Orazio et al. 2013; Farris et al. 2014). Gas may also be instrumental in deciphering the so-called final parsec problem (Begelman et al. 1980; Milosavljević & Merritt 2003; Armitage & Natarajan 2005), bringing MBHBs down to the orbital separations considered here. We consider such accreting binary systems and the possibility that emission from the gas bound to one MBH can be gravitationally lensed by the other, generating a detectable flare that may act as a unique identifier of the MBHB and disc system.

The range of binary orbital parameters of interest to this study is set primarily by observational constraints. We set a maximum binary separation by requiring that the entire orbital period of the binary be observed twice within the lifetime of a survey. While, as we discuss in Section 3, the detection of a single lensing flare may be sufficient for determining its origin, to be conservative, we require two successive observations of the lensing flare, allowing a minimal identification of periodicity. This motivates us to set an upper limit of  $\sim 10$  years on the observed binary orbital period, corresponding to binary separations of  $a \lesssim 0.01 \text{ pc } M_8^{1/3} (1+z)^{-2/3}$ , where  $z$  is the redshift of the MBHB host galaxy,  $M_8$  is the total binary mass in units of  $10^8 M_\odot$ , and we assume that the binary is on a circular orbit throughout (however, see Section 3.4). This upper limit on the binary separation is always within the approximate size of a

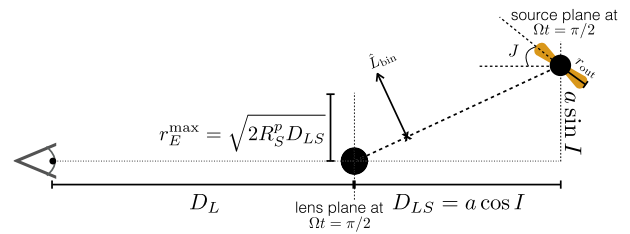


**Figure 1.** The lensing geometry at maximum magnification for a given binary inclination  $I$  and disc inclination  $J$ : viewed as the light emitting secondary BH passes behind the primary BH at a closest angular separation of  $a \sin I / D_L$ , at time  $\Omega t = \pi/2$ . Also labelled is the outer radius of the secondary accretion disc  $r_{\text{out}}$  and the *Einstein* radius of the primary BH at this moment in the orbit,  $r_E^{\text{max}}$ , where  $R_S^p$  is the Schwarzschild radius of the primary.  $\hat{L}_{\text{bin}}$  is the binary angular momentum unit vector.

gravitationally stable, circumbinary disc (Goodman 2003; Haiman, Kocsis & Menou 2009).

While we set no minimum binary period, we note that, observationally, a minimum will be set by the sample size of quasars that can be monitored in a survey. MBHBs with shorter orbital periods have shorter lifetimes and hence have a lower probability of detection (e.g. Haiman et al. 2009).<sup>1</sup> On the theoretical side, we treat the lens as a point mass and carry out all lensing calculations in the weak-field gravity limit. For very close binaries, however, one must take into account strong-field gravitational effects.

## 2.2 Lensing scales

Consider a binary with orbital period  $P$ , primary and secondary masses  $M_p$  and  $M_s$ ,  $M_s \leq M_p$ , total mass  $M \equiv M_p + M_s$ , and mass ratio  $q \equiv M_s/M_p$ , where the subscripts  $p$  and  $s$  refer to the primary and secondary BH, respectively, throughout. We study lensing of an emission region bound to the secondary BH by the primary BH, or vice versa. The lensing geometry for a snapshot of the binary orbit is depicted in Fig. 1.

Throughout we treat the lens as a point mass (we address this approximation in Section 2.5.). Whether the accretion disc may be treated as a point source depends on its physical size relative to the *Einstein* radius of the lens. The *Einstein* radius of the primary, when lensing the secondary, is,

$$r_E^p = \sqrt{2R_S^p a \cos I \sin \Omega t}, \quad (1)$$

where  $R_S^p$  is the Schwarzschild radius of the primary,  $I$  is the inclination of the binary plane to the line of sight,  $\Omega = 2\pi/P$  is the binary orbital angular frequency,  $a$  is the binary orbital separation given by  $\Omega$  and  $M$ , and the *Einstein* radius  $r_E^p$  is complex when the secondary passes in front of the primary. We have assumed that the distances to the source and to the lens  $D_L$  are equivalent since  $D_L \gg a$ .

From tidal truncation theory we know that the accretion flow around the secondary BH can be as large in extent as  $\eta(q/3)^{1/3}a$ , where  $\eta < 1$ . Because the *Einstein* radius grows more slowly with

<sup>1</sup> Combining the models of Haiman et al. (2009) for gas plus gravitational wave driven orbital decay and an AGN sample size of  $\sim 10^5$  (e.g. the Catalina Real Time Transient Survey; Drake et al. 2009; Djorgovski et al. 2010; Djorgovski et al. 2011; Mahabal et al. 2011), we estimate the binary period below which less than one MBHB is expected to be found. This minimum detectable MBHB period is  $P_{\min} \approx 79 \text{ d } M_8^{5/8} q_s^{3/8}$  or  $a \geq 8 \times 10^{-4} \text{ pc } M_8^{3/4} q_s^{1/4}$ .

separation, as  $\sqrt{a}$ , the projected size of the secondary accretion flow can be larger than the *Einstein* radius of the primary and, hence, for larger separation (longer period) binaries, we must treat the source as finite in size. We treat both the point source and finite-sized source cases below.

### 2.3 Point source

We first compute the lensing probability, time-scale, and time-dependent magnification of the source accretion disc, treating it as a point source. This is accurate for the highest energy emission that emanates from the accretion disc inner edge. The point-source case also serves as a comparison to the more general, finite-sized source case.

A significant lensing event occurs when the source passes within one *Einstein* radius of the lens. Hence, the probability of observing a lensing event, after observing the binary for an entire orbit, is the ratio of binary inclination angles for which the source falls within one *Einstein* radius of the lens to the total possible range of inclinations,

$$\mathcal{P}_s \sim \frac{2}{\pi} \sin^{-1} \left( \frac{r_E^{\max}}{a} \right) \approx 2 \frac{\mathcal{T}_s}{P},$$

$$\mathcal{P}_p = q^{1/2} \mathcal{P}_s, \quad (2)$$

where the subscripts  $s$  and  $p$  refer to the binary component that is being lensed,  $r_E^{\max}$  is the *Einstein* radius when the source is directly behind the primary ( $I = 0$  and  $\Omega t = \pi/2$  for the primary *Einstein* radius), and  $n_a \equiv a/R_S$  is the binary separation in units of the Schwarzschild radius of the total binary mass. In deriving equation (2) we have neglected a factor of  $(\cos I)^{-1/2}$ , which is near-unity for the cases considered here. Note that when  $n_a \rightarrow 2$ , emission from the secondary is strongly lensed at any binary inclination (though we would no longer be in the weak-field regime and relativistic ray tracing must be carried out).

We estimate the time-scale of a lensing event by calculating the fraction of an orbit for which the source lies within the *Einstein* radius of the lens. Assuming that the binary is inclined close enough to the line of sight for significant lensing to occur,

$$\mathcal{T}_s \sim \frac{1}{\pi} \sin^{-1} \left( \frac{r_E^{\max}}{a} \right) P \approx \frac{1}{\pi} \sqrt{\frac{2}{n_a}} (1+q)^{-1} P,$$

$$\mathcal{T}_p = q^{1/2} \mathcal{T}_s, \quad (3)$$

where again the subscripts  $s$  and  $p$  refer to the binary component that is being lensed. It is interesting to note that in the  $n_a \rightarrow 2$  limit mentioned above, the source is strongly lensed for the entire half-orbital period for which the source is behind the lens.

Fig. 2 plots the probabilities (dashed black lines) and lensing time-scales (orange lines) for a range of binary masses and periods amenable to observation through time-domain surveys. To compute time-scales and probabilities we choose mass ratios of  $q = 0.05$  and  $q = 0.5$  and a redshift of  $z = 1.03$  corresponding to the average of the samples of Graham et al. (2015a) and Charisi et al. (2016). For reference, the masses and periods of these MBHB candidates are overplotted as black circles. The delineation of the binary parameter space into finite-sized source (blue), point-source (white), and strong-field (red) regimes is discussed in more detail in the next section. We find that for MBHBs with masses and periods representative of those that can be identified in time-domain surveys, the probability of a lensing event (equation 2) is significant, ranging from  $\sim 1$  per cent chances for the smallest,

$10^5 M_\odot - 10^6 M_\odot$  MBHBs to 10s of percent for the highest mass  $\gtrsim 10^8 M_\odot$  binaries.

The magnification of a point source by a point mass is (Paczynski 1986)

$$\mathcal{M}_{\text{ps}} = \frac{u^2 + 2}{u\sqrt{u^2 + 4}}, \quad (4)$$

where  $u$  is the angular separation of source and point mass in units of the *Einstein* radius. For the orbiting secondary,

$$u_s = \mathcal{R}e \left\{ \frac{a}{r_E^p} \sqrt{\cos^2 \Omega t + \sin^2 I \sin^2 \Omega t} \right\}, \quad (5)$$

where  $\mathcal{R}e$  denotes the real part and  $r_E^p$  is given by equation (1). In the case that the secondary lenses the primary, we simply swap  $r_E^p$  with  $r_E^s$  and  $\Omega t$  with  $(\Omega t - \pi)$ . The total magnification of both lensing events is then found by inserting  $u = \mathcal{R}e\{u_s + u_p\}$  in equation (4). The binary inclination angle written in terms of the projected angle on the sky in units of *Einstein* radius is

$$\sin I = A \left[ \frac{\sqrt{4 + A^2}}{2A} - \frac{1}{2} \right]^{1/2}; \quad A \equiv N_E^2 \frac{2R_S^p}{a}, \quad (6)$$

where  $N_E$  is defined to be the inclination angle measured in units of the maximum *Einstein* radius of the primary,  $r_E^{\max}$  (see discussion below equation 2). Equivalently,  $N_E$  is the number of *Einstein* radii separating source and lens at closest approach. In the limit of small  $I$ ,

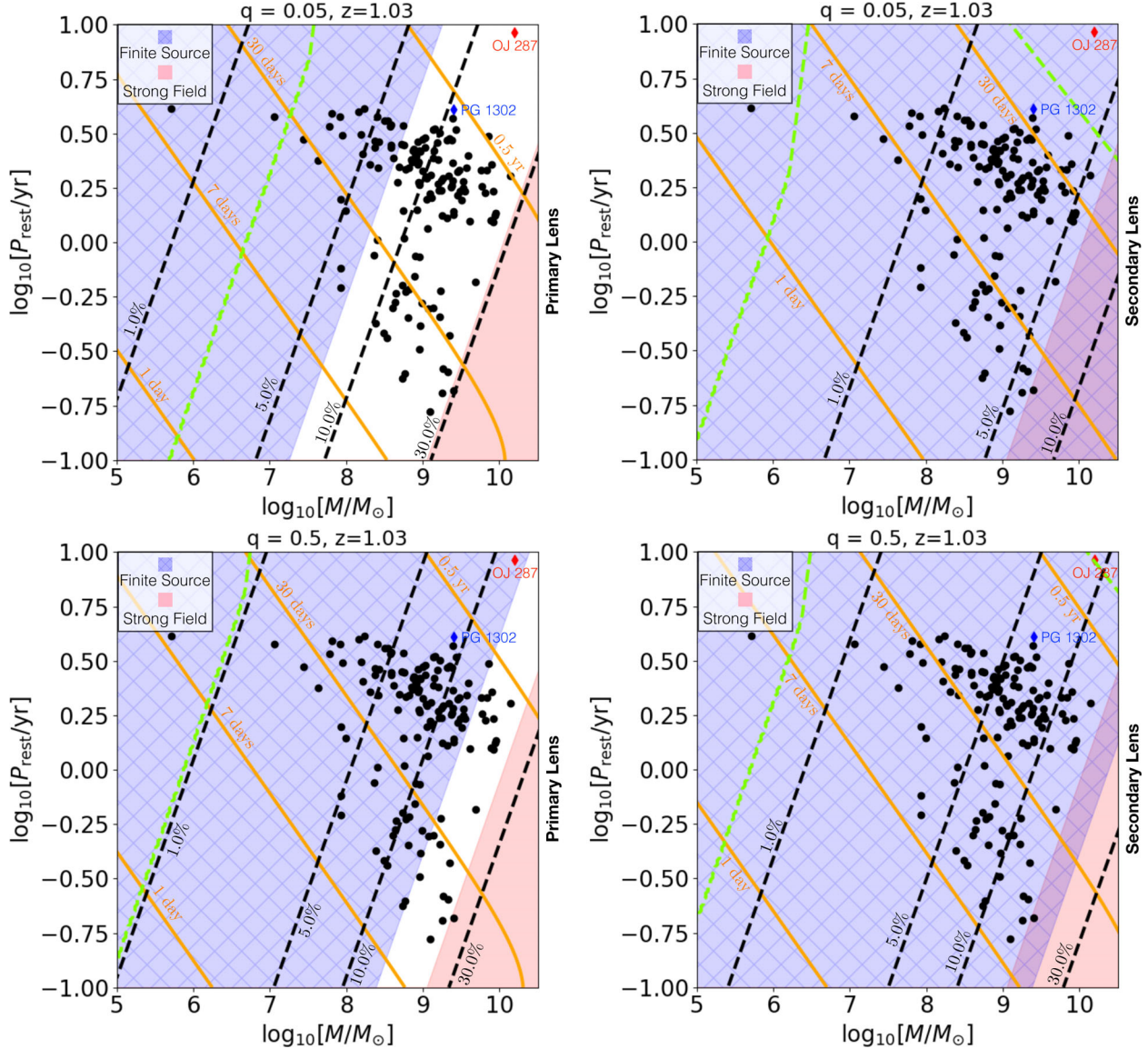
$$\sin I \approx N_E \sqrt{\frac{2R_S^p}{a}}. \quad (7)$$

Fig. 3 uses equations (4) and (5) to compute sample light curves of observed emission from a steadily accreting secondary in a binary with a total mass of  $10^9 M_\odot$  and a period of 4 years. We assume the case of Doppler-boost-induced broad-band periodicity: we allow both primary and secondary BH to emit at the same total brightness and combine the competing contributions from the relativistic Doppler boost, each multiplied by the appropriate lensing magnification (see D’Orazio et al. 2015b). In each panel we plot light curves for different binary inclinations to the line of sight. Note that, because the total emitted light is split between the two binary components, the maximum magnification of a lensing flare is smaller than if we assumed all light came from one component (compare the peaks in Fig. 3 with the corresponding values in Fig. 4).

In the left panel of Fig. 3, we assume a binary mass ratio of  $q = 0.05$ , then for  $N_E \lesssim 1.5$  ( $\sim 11^\circ$  from edge on) we find an appreciable lensing flare as the secondary passes behind the primary, reaching a factor of  $\sim 1.6$  in magnification when  $N_E \rightarrow 0.5$  ( $\sim 4^\circ$  from edge on). In the right panel we consider a larger,  $q = 0.5$ , mass ratio binary. In this case we see two lensing flares. The first is similar to the more extreme mass ratio case, corresponding to when the secondary passes behind the primary, and a second flare now occurs as the primary (if it is accreting) passes behind the secondary. In both cases, the lensing flares disappear as the binary inclination increases, first for the lensed primary and then for the lensed secondary, leaving only the sinusoidal Doppler-boost signal (dashed-blue line) which then also disappears as the binary inclination approaches face on (dot-dashed black line).

We see only a small secondary flare in the more extreme mass ratio case (right panel of Fig. 3) because, for small  $u$ ,  $\mathcal{M}_{\text{ps}}$  (equation 4) goes as  $1/u$  and  $u \propto 1/r_E \propto M^{-1/2}$ , then the maximum lensing





**Figure 2.** Contours in orbital period and binary mass space of the lensing time-scale (orange lines) and probability that the source centre passes within one *Einstein* radius of the lens, after one orbital period of observation (black-dashed lines). The left (right) column is for the primary (secondary) lensing the secondary (primary) accretion disc. The top (bottom) row assumes a mass ratio of  $q = 0.05$  ( $q = 0.5$ ). The parameter space is delineated into three regions where different lensing effects dominate. In the blue shaded region, finite-sized source effects are important due to the large relative size of the source accretion disc to the *Einstein* radius of the lens. The red-shaded region is where strong-field gravitational effects become important, and the non-shaded region is where point-lens and point-source approximations are valid. At separations larger than those delineated by the green-dashed line, the disc may be truncated by self-gravity rather than tidal forces. The black circles are MBHB candidates identified in time-domain surveys as periodically varying quasars (Graham et al. 2015a; Charisi et al. 2016). All calculations assume  $z = 1.03$ , the average redshift of the plotted MBHB candidate sample.

magnification by the secondary BH (second, smaller flare) is related to the maximum lensing magnification by the primary BH (first, larger flare) by  $\sqrt{q}$ . Hence the binary with  $q = 0.05$  does not exhibit a significant secondary flare as this flare is  $\sim 4.5$  times smaller than the primary flare. The  $q = 0.5$  (right panel) binary does exhibit a secondary flare as its magnification is only  $\sim 1.4$  times smaller than the primary flare.

A key feature of the light curves in Fig. 3 is the time-order of the flares and their magnitudes: a high-magnification flare followed by a lower magnification flare (or no detectable flare at all). For a Doppler-boost plus lensing light curve this time and magnitude ordering always occur unless the primary is emitting a significantly

larger fraction of the light in the observing band. This is because of the following reasons.

- (i) The more massive primary generates a larger magnification of the secondary accretion disc than in the opposite scenario.
- (ii) Because the secondary is expected to accrete at a higher rate (Farris et al. 2014) and moves faster in its orbit, it dominates the sinusoidal Doppler-boost signature. Hence, the sinusoidal part of the light curve in Fig. 3 is increasing after the secondary is lensed, when the secondary is moving towards the observer.

The above two points imply that the secondary passes behind the primary during the increasing flux portion of the sinusoidal light

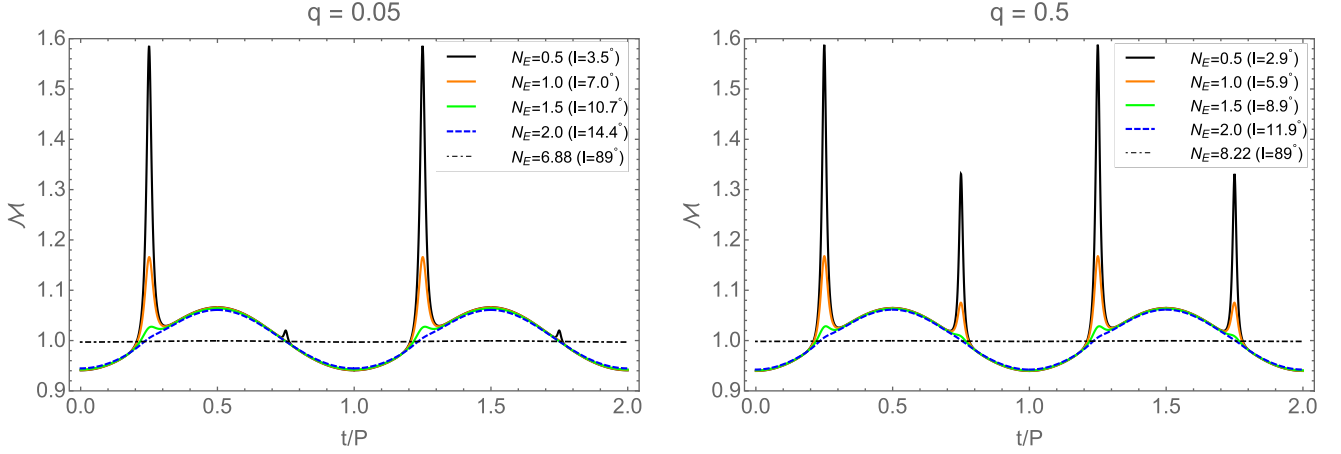


**Figure 3.** Magnification of Doppler-boosted and lensed emission from primary and secondary point-source emission for binary parameters  $(P, M) = (4.0 \text{ yr}, 10^9 M_\odot)$  and for the stated values of the binary orbital inclination, listed in the legend in terms of  $N_E$  defined in equation (7). Both primary and secondary discs are assumed to emit at the same brightness. The first lensing flare is due to lensing of the secondary accretion disc by the primary and the second lensing flare is due to lensing of the primary accretion disc by the secondary. The inclination of the binary that could generate the orange light curve has probability given by the black-dashed lines in Fig. 2. The black light curve has a lower probability of occurring, but would be easier to discover.

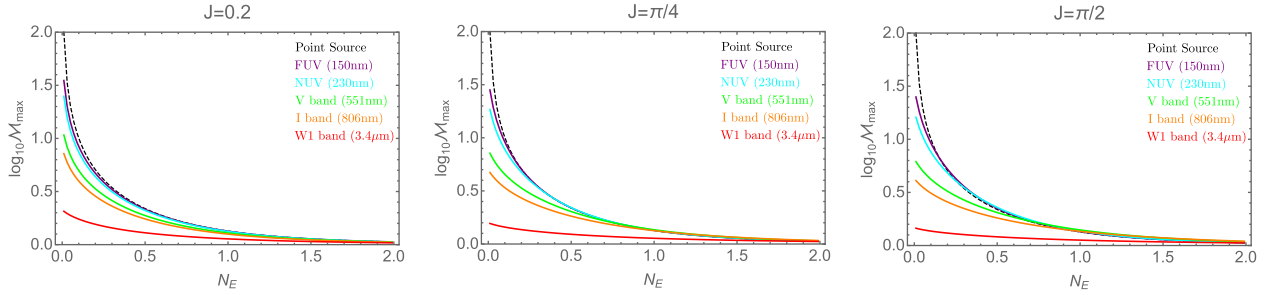


**Figure 4.** Magnification of the secondary emission, at closest approach to the lens, plotted against the inclination of the binary to the line of sight in units of the number of *Einstein* radii that make up the angular separation of source and lens at closest approach,  $N_E$ . The finite size of the source is set by the observed wavelength. Shorter wavelength radiation comes from a smaller inner region of the disc and so approaches the result of the point-source calculation (dashed-black line). The binary mass and period set the inclination angle in radians (see equation (7)). From left to right we tilt the accretion disc from a nearly edge-on ( $J = 0.2$ ) to a face-on inclination ( $J = \pi/2$ ).

curve, and hence the larger flare occurs here. For flares that accompany broad-band periodicity due to accretion variability, the time-ordering of flares relative to the light curve minima and maxima is not constrained. This ordering could inform us how accretion proceeds on to the binary components.

Fig. 2 displays lensing time-scales and probabilities but does not show the maximum lensing magnification as a function of binary mass and period. This is because magnification depends solely on the closest angular approach of the secondary and primary on the sky ( $u$ ), and hence depends only on the binary inclination to the line of sight. Writing the inclination in terms of angular *Einstein* radii  $N_E$  (equation 7), the solid black line in Fig. 4 shows the maximum magnification of the secondary point source as a function of  $N_E$ . For example, when  $N_E = 1.0$ ,  $\mathcal{M} \approx 1.3$ , or when  $N_E = 0.5$ ,  $\mathcal{M} \approx 2.2$  (larger than seen in Fig. 3 because the Doppler calculation assumes that each binary component contributes equally to the total brightness of the system). The role of binary mass and period in the point-source case is to give physical units (in radians) to the inclination in units of angular *Einstein* radii. This is exactly the information portrayed by the probability contours in Fig. 2. A larger binary orbital separation (larger binary period and smaller mass) means that a smaller range of binary inclinations corresponds to the same inclination (and hence maximum magnification) in units of *Einstein* radii.

## 2.4 Finite source

The emitting, lensed accretion disc can no longer be treated as a point source if its angular extent is of order the *Einstein* radius of the lensing BH,

$$\rho(\lambda) \equiv \frac{r_d(\lambda)}{r_E} \approx \frac{1}{\sqrt{2n_a}} \frac{r_d(\lambda)}{R_s} \gtrsim 1, \quad (8)$$

where again  $n_a$  is the binary separation in units of the Schwarzschild radius of the total binary mass and  $r_d(\lambda)$  is the wavelength-dependent size of the accretion disc.

We model  $r_d(\lambda)$  by assuming a steady-state alpha disc where absorption opacity dominates scattering. Then using the standard steady-state disc photosphere temperature (see equation 13 below) for  $r \gg 6GM/c^2$ , we solve for the radius where the accretion disc spectrum peaks at wavelength  $\lambda$ . Dividing by the *Einstein* radius of primary and secondary, respectively,

$$\begin{aligned} \rho^s(\lambda) &\approx 1.1 \frac{q^{2/3}}{(1+q)^{1/6}} \left( \frac{150}{n_a} \right) \left( \frac{\lambda}{230 \text{ nm}} \right)^{4/3} \left( \frac{\epsilon^{-1} \eta M}{10^9 M_\odot} \right)^{-1/3} \\ \rho^p(\lambda) &= q^{-7/6} \rho^s(\lambda), \end{aligned} \quad (9)$$

where again superscripts  $s$  and  $p$  refer to the binary component being lensed,  $\epsilon$  is the disc accretion rate in units of the Eddington rate, and  $\eta$  is the accretion efficiency factor.

The size of the disc is limited at the inner edge by the innermost stable circular orbit (ISCO) of the accreting BH. At the outer edge the disc size is limited by tidal truncation or possibly by gravitational or ionizational instability. Assuming for now that tidal truncation dominates (which it does for smaller binary separations, where finite-sized source effects first become important, and where the probability of lensing is larger), we explore the importance of treating the source as having a finite-size.

For the secondary disc, the tidal truncation radius is  $r_{\text{out}}^s \approx 0.27q^{0.3}a$ , and for the primary  $r_{\text{out}}^p \approx 0.27q^{-0.3}a$  (Papaloizou & Pringle 1977; Paczynski & Rudak 1980; Roedig, Krolik & Miller 2014). Then we may estimate the largest accretion disc sizes at any wavelength as

$$\begin{aligned}\rho_{\text{max}}^s &\approx 1.0 \left( \frac{n_a}{27.5} \right)^{1/2} q^{0.3} \sqrt{1+q} \\ &\approx 1.0 \left( \frac{M}{10^9 M_\odot} \right)^{-1/3} \left( \frac{P}{4.0 \text{ yr}} \right)^{1/3} q^{0.3} \sqrt{1+q}, \\ \rho_{\text{max}}^p &= q^{-1.1} \rho_{\text{max}}^s.\end{aligned}\quad (10)$$

The peak wavelength of emission at the accretion disc outer edge can be found by equating  $r_{\text{out}}$  and  $r(\lambda)$  used in equation (9) above,

$$\begin{aligned}\lambda_{\text{out}}^s &= 209 \text{ nm} \left( \frac{M}{10^9 M_\odot} \right)^{-1/4} \left( \frac{P}{4.0 \text{ yr}} \right)^{1/2} \left( \frac{\eta}{\epsilon} \right)^{1/4} \\ &\quad \times q^{9/40} \sqrt{1+1/q} \\ \lambda_{\text{out}}^p &= q^{1/20} \lambda_{\text{out}}^s.\end{aligned}\quad (11)$$

The blue shaded regions of Fig. 2 show where tidal truncation predicts that finite-sized source effects become important using equations (10). We see that the finite size of either primary or secondary accretion disc can become important for fiducial binary masses, periods, and mass ratios considered here and also at important observing wavelengths via equation (11). Accretion discs around lower mass and longer period binaries are lensed as finite-sized sources unless disc instability such as self-gravity truncates the disc to a smaller size than the tidal truncation radius. Also, lensing of the primary accretion disc by the secondary is more likely to occur in the finite source regime.

Note that  $\rho_{\text{max}}$  is an increasing function of binary separation. This follows because a wider binary allows the discs around each BH to be truncated at a larger physical distance from the BH that grows linearly with the orbital separation, whereas the *Einstein* radius grows with the square root of the orbital separation. The interpretation of  $\rho_{\text{max}}$  as an indicator of the importance of finite-sized source effects then follows only if the disc is stable out to the truncation radius. This assumption could break down at sufficiently large binary separations.

As an estimate of where instabilities could truncate the disc to smaller sizes than required by tidal truncation, we calculate the mini-disc gravitational instability radii assuming steady-state alpha-disc solutions [see equations (12)–(16) of Haiman et al. (2009)]. The binary parameters for which the tidal and self-gravity truncation radii are equal are delineated as a green-dashed line in each panel of Fig. 2. This shows that the smallest and largest mass and longest period binaries could have mini-discs that are truncated by gravitational instability, causing them to act as point sources rather than the finite-sized sources predicted by tidal truncation. We note, however, that this instability radius is highly uncertain as it assumes a specific steady-state disc model. We continue our analysis using the more robust tidal truncation radii, but wish only to point out that

self-gravity truncation could become important for determining the lensing regime for the binary parameters of interest.

To compute the wavelength-dependent magnification of the secondary’s accretion disc, we take into account the radius and wavelength-dependent flux given by steady-state alpha-disc models,

$$F_\nu(r) = \pi B_\nu[T(r)], \quad (12)$$

where  $B_\nu$  is the Planck function and  $T(r)$  is the radius-dependent effective temperature of the disc photosphere, given by balancing viscous heating with radiative cooling,

$$\sigma T^4 = \frac{3GM\dot{M}}{8\pi r^3} \left[ 1 - \left( \frac{r_{\text{ISCO}}}{r} \right)^{1/2} \right]. \quad (13)$$

Using polar coordinates  $(u, v)$  centred on the lens, and  $(r, \phi)$  centred on the source, the magnification, in a given observing band, is

$$\mathcal{M}_\nu^{FS} = \frac{\int_0^{2\pi} \int_0^\infty F_\nu(u', v') \mathcal{M}_{\text{PS}}(u') u' du' dv'}{\int_0^{2\pi} \int_0^\infty F_\nu(u', v') u' du' dv'}, \quad (14)$$

where  $\mathcal{M}_{\text{PS}}$  is the point-source magnification (equation 4). To write  $F_\nu$  in terms of lens-centred coordinates  $(u, v)$  we use that

$$r_*^2 = (u_0^2 + u^2 - 2u_0 u \cos(v - v_0)) r_E^2,$$

$$r = r_* \sqrt{\cos^2 \phi + \frac{\sin^2 \phi}{\cos^2(\pi/2 - J)}},$$

$$\sin \phi \equiv \frac{u \sin v - u_0 \sin v_0}{\sqrt{(u \sin v - u_0 \sin v_0)^2 + (u \cos v - u_0 \cos v_0)^2}}, \quad (15)$$

where  $(u_0, v_0)$  is the position of the secondary in lens-centred, polar coordinates:  $u_0$  is given by equation (5) in units of *Einstein* radii and  $v_0 = \tan^{-1}[\sin I \tan \Omega t]$ ;  $J$  is the inclination of the source disc to the line of sight (see Fig. 1), and  $\phi$  is the polar coordinate in the disc-centred frame. To evaluate equation (14), we set  $F_\nu = 0$  when  $r$  is less than the ISCO radius or when  $r$  is greater than the truncation radius discussed above.

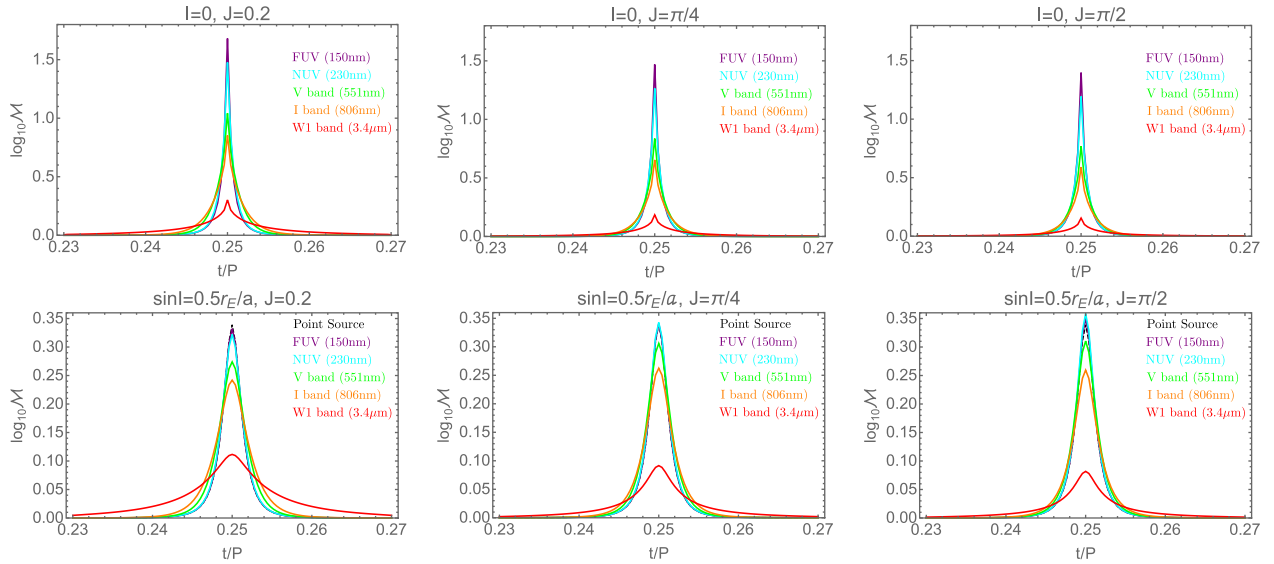
#### 2.4.1 Wavelength-dependent effects

Fig. 5 plots the wavelength-dependent, finite-sized source lensing light curves, focusing on the flare produced by lensing of the secondary accretion disc. The top row is for an edge-on binary inclination while the bottom inclines the binary to  $\sim 0.7$  from edge on, corresponding to a minimum sky separation of  $0.5r_E^p$  ( $N_E = 0.5$ ). Both rows vary the inclination of the accretion disc source to the line of sight from nearly edge on ( $J = 0.2$ ) to face on ( $J = \pi/2$ ).

In each of the panels we have assumed a binary with total mass  $10^6 M_\odot$ , mass ratio of  $q = 0.1$ , and an orbital period of 4 years. According to equation (11), this places the peak wavelength of emission at the tidal truncation radius of the secondary at  $\lambda_{\text{out}} = 2.3 \mu\text{m}$ , in the near-infrared (IR). The tidal truncation radius of the secondary accretion disc is  $r_{\text{out}}^s \sim 0.14a$  corresponding to  $\rho_{\text{max}}^s = 11.3$ , hence finite-sized source effects should be prominent in the optical and UV wavelengths, approaching the point-source case for far-UV and X-ray wavelengths.

In Fig. 5 we plot the simulated lensing flare in far-ultraviolet (FUV; 150 nm) to red optical (*I* band; 806 nm) and IR (*W1* band; 3.4  $\mu\text{m}$ ). Because the disc is hotter at its centre, and hence emits shorter wavelength radiation there, the FUV represents the smaller inner region of the secondary disc while the optical/IR represents the larger outer portion of the disc. The result, seen in Fig. 5, is that the optical/IR lensing is spread out, beginning earlier, ending





**Figure 5.** Zoomed-in light curves for multi-wavelength observations of a lensed, finite-sized accretion disc around the secondary BH. Here we fix the binary to have total mass  $10^6 M_\odot$ , mass ratio of  $q = 0.1$ , and an orbital period of 4 years. This sets the plotted time frame to be approximately two months. Each column, from left to right, assumes a different value of the secondary accretion disc inclination to the line of sight, from nearly edge on ( $J = 0.2$ ) to face on ( $J = \pi/2$ ). The top row assumes an edge-on binary orbital inclination ( $I = 0$ ,  $N_E = 0$ ), and the bottom row assumes a binary orbit inclined such that the projected sky separation of the BHs at closest approach is half of an *Einstein* radius ( $\sin i \approx 0.5r_E/a$ ,  $N_E \approx 0.5$ ). For the binary considered here this corresponds to an  $\sim 0.7$  orbital inclination to the line of sight. We assume that the source accretion disc emits the spectrum of a standard steady-state accretion disc.

later, and reaching a lower peak magnification than the flares at shorter wavelengths. The shorter wavelength, NUV, and FUV flares approach the shape and peak magnification predicted by the point-source case.

The finite-sized source lensing depends not only on the size of the source, but also on the shape. The inclination of the disc to the line of sight changes the shape of the emitting region from a large face-on disc at  $J = \pi/2$  to a more narrow ellipse constricted in the direction perpendicular to motion across the sky (however, see Section 3.4). The result is that more edge-on discs approach more closely the point-source case because the elongated edge-on discs are less smeared out over the  $u = 0$  caustic. This can be seen in Fig. 5 where, from left to right, the disc is inclined from nearly edge on to face on and the redder wavelength light curves decrease in peak magnitude. The width of the lensing curve does not change greatly because we only allow the disc to be inclined to the line of sight. Future parameter studies could allow a more general parametrization of the accretion disc shape; this could result in a larger range of possible flare durations.

We investigate the effect of changing binary inclination angle by comparing the top and bottom rows of Fig. 5. Just as for the point-source case depicted in Fig. 3, increasing the binary inclination away from the line of sight decreases the peak magnitude of amplification. In the finite-sized source case, increasing the binary inclination also rounds the light curve from a cuspy spike at edge-on inclination, caused by a direct crossing of the source through the  $u = 0$  caustic, to a rounder flare when the source passes just above or below the caustic. In the bottom row, for which the binary is inclined from edge on, we have drawn the point-source case as a dashed black line. We do not draw the point-source light curve for the edge-on binary because it results in an infinite magnification. This infinite magnification is smeared out for the finite-sized source cases plotted in Fig. 5.

For a binary inclined to the line of sight ( $I \neq 0$ ), Fig. 5 shows that the magnification of the shorter wavelength emission does

not change appreciably with  $J$ , and is similar to the point-source case. The longer wavelength emission, however, is magnified over a shorter time-scale as  $J$  is increased towards face on. This shows that binary orbital inclination affects different wavelength emission differently in the finite-sized source case. Generally, if the extended source, at a given wavelength, has components that intersect the lensing caustic, these wavelength components are affected by finite-sized source effects; it is the shape of the emitting region on the sky, and hence  $J$ , that determines whether or not different regions of the disc cross the  $u = 0$  caustic.

Fig. 4 shows how the maximum magnification in the finite-sized source case compares to that of the point-source case at different wavelengths, as a function of binary inclination angle. As expected, the finite-sized source and point-source cases are identical for large binary inclination, but quickly diverge once the binary inclination places the source within one *Einstein* radius of the lens. As the binary inclination approaches edge on, the point-source case approaches infinite magnification while progressively longer wavelength observations exhibit lower peak magnification as explained above.

Finally, we note that Figs 4 and 5 only consider finite-sized source effects for one set of binary mass, mass ratio, and orbital period. The primary difference in changing binary parameters is the mitigation of finite-sized source effects for more closely separated MBHBs (and widely separated MBHBs if self-gravity truncates discs around each BH). This is apparent from equation (10) and Fig. 2. Changing the binary parameters will also relabel the important wavelengths for finite-sized source effects determined through equation (11).

## 2.5 Strong-field effects

Thus far, we have treated the lens as a point mass in the weak-field gravity limit. We briefly address the validity of this assumption.

Strong-field effects can generate relativistic images not captured in this analysis; however these images are highly

demagnified compared to those considered here in the weak-field limit. For the MBHB system, the ratio of weak-field and relativistic magnifications for a Schwarzschild BH is  $\mathcal{M}_{\text{wf}}/\mathcal{M}_{\text{rel}} \approx 83(a/R_s)^{3/2}$ , where  $R_s$  is the Schwarzschild radius of the lens (Bozza et al. 2001).

In the strong-field limit, one must also take into account gravitationally induced time delays that could shift the arrival time and shape of the lensing signal. For the binary periods considered here, the largest effect, the Shapiro delay (Shapiro 1964; Meiron, Kocsis & Loeb 2017), is small compared to the lensing time-scale computed in equation (4),

$$\frac{\delta t_{\text{Shap}}}{T_s} \approx 0.006 \left( \frac{M}{10^8 M_\odot} \right)^{2/3} \left( \frac{P}{\text{yr}} \right)^{-2/3}, \quad (16)$$

where we have used a minimum inclination corresponding to the source aligned with the event horizon radius of the lensing primary. The Shapiro delay becomes an  $\sim 10$  per cent effect for the relativistic systems near merger studied in Schnittman et al. (2017) and Haiman (2017).

Hence, at closer binary orbital separations ( $n_a \lesssim 10$ ), future work must carry out relativistic ray tracing in the binary spacetime (e.g. Schnittman et al. 2017). For the purposes of this study, however, the point mass lens is a good approximation.

### 3 DISCUSSION AND CONCLUSION

#### 3.1 Lensing as a unique signature of MBHBs

A lensing signature is required by relativity alone, provided the binary is accreting and at a low orbital inclination to the line of sight. Furthermore, a self-lensing flare can be distinctly distinguished from intrinsic AGN flaring and variability by a few unique features. In the point-source case, at binary separations less than  $\sim 100R_s$  (for the secondary and  $q = 0.1$ ), the amplification caused by lensing is periodic and achromatic, identical in all wavelengths. Wavelength independent periodic flaring would be a smoking-gun signature of self-lensing in the point-source regime. Practically, because intrinsic emission from the lensed source is likely not identical at all wavelengths, a sufficient understanding of the unlensed light curve must be modelled from data surrounding the flare in order to confirm a wavelength invariant amplification.

To elaborate further, consider a representative MBHB candidate from Fig. 2. For such a system, the probability of the secondary passing within one *Einstein* radius of the primary is  $\sim 10$  per cent. The maximum magnification in the point-source case is 1.32, corresponding to a 32 per cent variability amplitude. Comparatively, the average amplitude of variability in the combined sample of MBHB candidates from Graham et al. (2015a) and Charisi et al. (2016) is  $16 \pm 8$  per cent, smaller than, but comparable to, the amplification predicted here. This is encouraging for detectability of such lensing flares. However, the amplification of 1.32 assumes that all of the light is emitted by the lensed source. This is likely not the case. As we discussed at the end of Section 2.3, this magnification factor drops to  $\sim 1.16$  when it is assumed that the secondary and the primary contribute equally to the total emission (Fig. 3). If an equal amount of light is also being emitted by the circumbinary disc, then this total magnification drops to 1.11. Furthermore, the relative contribution from each light emitting component at different wavelengths causes the lensing signature to have a different peak magnification at these different wavelengths, even in the point-source case. While this complicates identification of a lensing

signature, it acts as a probe of the spectral energy distributions of the light emitting components of the MBHB system.

We note further that we have only discussed the most probable strongly lensed events, where the source passes within an *Einstein* radius of the lens at closest approach (or half of this in Figs 3 and 5). Hence, lower probability events generate higher magnification flares than those plotted in Fig. 3 and could be easier to identify observationally. Generally, there is a trade off between ubiquity and ease of identification.

In the case of a finite-sized source, the flare is no longer intrinsically achromatic in peak magnitude, but does, barring any reprocessing or light-echo effects, reach peak magnitude at the same time and share similar full width at zero maxima for all wavelengths (The pulse shapes in Fig. 5 all share nearly identical pulse times from turn on to turn off.). If detection of the orbital Doppler boost is not possible, this flare-timing coincidence plus the simultaneous modelling of the accretion disc emission profile and the wavelength-dependent lensing-flare shape could be carried out in order to differentiate the lensing event from other AGN flaring activity. If, for example, such intrinsic AGN flares are generated by propagating disturbances in the accretion flow, they will exhibit wavelength-dependent time lags, not seen in a lensing flare.

As suggested by Fig. 3, if the orbital inclination of the binary is small enough to detect a lensing flare, then there will also be periodic modulation of the light curve due to the relativistic Doppler boost. If the periodic variation from the relativistic Doppler boost is detected, more constraints can be placed on the system. In this case, a known mass and spectral index, in addition to the inferred binary period, yield the Doppler magnification up to the unknown binary inclination and mass ratio (e.g. D’Orazio et al. 2015b). Then the lensing flares can be identified by their specific position at the average flux locations of the Doppler modulation (e.g. Fig. 3) and further constrain the binary mass ratio, inclination, and the projected source shape (parametrized by  $J$  here). A detection of a flare with appropriate properties (width, achromaticity) at the average flux location of the Doppler sinusoid could even allow identification of such MBHB self-lensing systems without the need for multiple cycles, lessening the period requirements discussed in Section 2.1.

If lensing events from both primary and secondary can be detected along with the Doppler-boost modulation, then the relative brightness of primary and secondary accretion discs can be discerned in the given observing band. The BH that dominates the orbital Doppler modulation (usually the faster moving, brighter secondary) is lensed during the rising flux portion of the Doppler light curve and the sub-dominant Doppler contributor is lensed during the falling flux portion. Whether the dominant or sub-dominant emission is generated by the secondary or primary can be discerned from the relative widths and magnifications of each lensing flare, smaller by a factor of  $\sqrt{q}$  for lensing by the secondary.

Equations (10) show that for both BH discs to enter the finite source regime the binary separation must be

$$a_{\text{fs}} \gtrsim 27.5 R_s q^{-0.6} (1+q)^{-1}. \quad (17)$$

For both to be in the point-source regime the binary separation must satisfy

$$a_{\text{ps}} \lesssim 27.5 R_s q^{1.6} (1+q)^{-1}. \quad (18)$$

Hence, for a mass ratio of  $q = 0.1$ , the binary must have separation above  $\sim 100R_s$  for both primary and secondary discs to act as finite-sized sources, or separations below 0.6 Schwarzschild radii for both to act as point sources.



For binary separations  $\sim 100R_s$ , the secondary accretion disc is effectively a point source when lensed by the primary while the primary accretion disc must be treated as a finite-sized source when lensed by the secondary. This scenario could prove useful for identifying the lensing system with the more highly magnified and achromatic lensing of the secondary disc and then using the finite source lensing of the primary disc to learn about the accretion flow on to the primary.

Because  $a_{ps}$  is small enough that the primary and secondary discs may be truncated behind the ISCO, we conclude that the case where both accretion discs act as a point source is only achieved for near-unity mass ratios, very close to merger.

### 3.2 The MBHB population

At the time of writing there are  $\sim 150$  quasars identified as MBHB candidates by optical periodicity (Lehto & Valtonen 1996; Graham et al. 2015a,b; Liu et al. 2015; Charisi et al. 2016; Li et al. 2016; Zheng et al. 2016; Dorn-Wallenstein, Levesque & Ruan 2017; Li et al. 2017). Some of these have corroborating UV (D’Orazio et al. 2015b), IR (Jun et al. 2015; D’Orazio & Haiman 2017), and radio (Pursimo et al. 2000) time series data as well. Fig. 2 plots these candidates in period versus total binary mass space. According then to Fig. 2, at least  $\sim 7$  (5 per cent) of these candidates should exhibit self-lensing flares. While we have not carried out a rigorous search for such flares in the known candidate light curves, we note that, by eye, none exhibits the expected behaviour. We do not claim any discrepancy. However, we discuss why one might expect to find fewer lensing candidates in the existing sample than predicted by our calculations. We further discuss the implications of this for MBHB candidates and future searches.

First of all, the MBHB candidates found by Graham et al. (2015a) and Charisi et al. (2016) could be in tension with upper limits on the gravitational wave background (GWB) measured by the pulsar timing arrays (PTAs; Sesana et al. 2017). The present version of the work by Sesana et al. (2017), however, overestimates the mass of the MBHB candidates by a factor of  $\sim 4$  (Alberto Sesana and Zoltán Haiman, private communication). This mass overestimate may remove any tension with the GWB entirely. Any remaining discrepancy between the GWB and the known MBHB candidates, however, could mean that some of the candidates are manifestations of red-noise rather than true periodicity or resultant from non-MBHB induced periodicity due to, for example, scaled up versions of the quasi-periodic oscillations observed in micro-quasars (e.g. Remillard & McClintock 2006). We note that because self-lensing is more probable for the higher mass binaries, which generate a stronger PTA signal, preferential removal of the high-mass MBHB candidates helps even further to satisfy both the lensing and the PTA constraints. Future constraints using both the GWB and lensing statistics will help to vet the population of EM-identified MBHBs.

Even if all of the known MBHB candidates are real, and consistent with GWB measurements, the Graham et al. (2015a) and Charisi et al. (2016) studies may not have found the MBHBs which exhibit periodic flaring. This is because the selection processes used to identify periodic light curves preferentially pick out sinusoids. Lensing events in the Graham et al. (2015a) and Charisi et al. (2016) samples may have simply been discarded due to this bias. Hence, we point out that it is crucial that present and future time-domain surveys search for periodicity that may not necessarily be sinusoidal, but spiky as in the case of the self-lensing flares calculated here.

Finally, we note that some lensing flares may be at too low a magnification to be picked out from the data by eye. This could be due to flux contributions from components of the MBHB system that are not being lensed. Exploration of this possibility requires a more careful search in the existing MBHB candidate light curves. We leave this for a separate study.

The probability calculation of equation (2), plotted in Fig. 2, assumes a flat prior on the inclination of the binary orbit to the line of sight. If, however, a set of MBHB candidates is selected by identification of periodicity in AGN light curves due to the relativistic Doppler boost, the conditional probability of observing a lensing event increases. This is because observation of the Doppler boost restricts the range of possible binary inclinations.

To compute this conditional probability of lensing given an observed Doppler boost, we compute the range of orbital inclinations available to a binary given that it has been identified as a Doppler-boost candidate. For a given Doppler-boost MBHB candidate one has a measurement of  $n_a$  through the measured binary orbital period and mass, the amplitude of variability  $A_{\text{obs}}$ , and the spectral slope in the observing band  $\alpha$ . The binary mass ratio and orbital inclination are unknown but are related to each other and the measured parameters by

$$I(q) = \cos^{-1} \left[ (1+q) \frac{A_{\text{obs}}}{3-\alpha} \sqrt{n_a} \right], \quad (19)$$

to order  $v/c$  (see D’Orazio et al. 2015b) and where we have assumed that only the secondary is emitting light. For measured values of  $n_a$ ,  $\alpha$ , and  $A_{\text{obs}}$ , we can calculate the range of possible binary orbital inclinations from the range of mass ratios. We require as before that a significant lensing event be one that brings the source and lens within one *Einstein* radius of each other  $I \leq \sin^{-1} [\sqrt{2/n_a}]$  (equation 7). But now, instead of comparing this range of inclination angles to the full unrestricted  $\pi/2$  (equation 2), we take into account a smallest  $I(q=1)$  and largest  $I(q=0)$  possible binary inclination set by the Doppler-boost observation. Then the increased probability of lensing is

$$\mathcal{P}(L|D) \approx \frac{\sin^{-1} [\sqrt{2/n_a}] - \text{Re}\{I(q=1)\}}{\text{Re}\{I(q=0)\} - \text{Re}\{I(q=1)\}}. \quad (20)$$

We plot this probability as a function of binary separation and the spectral slope-dependent Doppler-boost amplitude  $A_{\text{obs}}/(3-\alpha)$  in Fig. 6. The upper-right grey region of Fig. 6 labelled ‘No Doppler Solutions’ is where the  $\alpha$ -scaled Doppler-boost amplitude is not achievable given the binary separation (no matter the orbital inclination or mass ratio). The lower-left blue region labelled ‘Weak Magnification’ is where the combination of  $A_{\text{obs}}/(3-\alpha)$  and  $n_a$  implies a binary inclination that is larger than that required for significant lensing, for any binary mass ratio. In between these two disfavoured regions we plot contours of the conditional probability (equation 20). As expected, the larger the observed Doppler-boost amplitude, the more narrow the allowed binary inclinations and the higher the conditional probability of lensing.

As an example of the utility of this calculation, we plot the position of the known Doppler-boost MBHB candidate PG 1302 in Fig. 6. We use the measured values of  $\alpha = 1.1$  and  $A_{\text{obs}} = 0.14$  in the optical and the range of separations given by the binary masses consistent with the Doppler-boost scenario  $M = 10^9 - 10^{9.4} M_\odot$  (D’Orazio et al. 2015b). It is interesting to note that PG 1302 falls in the allowed lensing regime. If the Doppler-boost interpretation is correct for PG 1302, then there is an  $\sim 30$  per cent chance for PG 1302 to have hosted a lensing flare. Because PG 1302 does not exhibit a lensing flare, however, further analysis could be used to

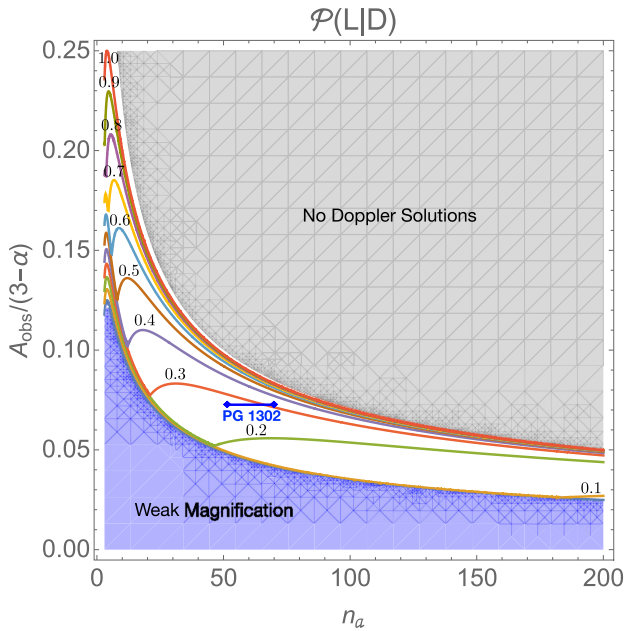


**Figure 6.** The probability of a lensing event (of the secondary accretion disc) given that the Doppler boost is observed (labelled contours). The Doppler-boost signature has modulation amplitude  $A_{\text{obs}} \equiv \Delta F_{\nu}/F_{\text{max}}$  for a binary with scaled separation  $n_a \equiv a/R_S$  and observed with spectral index  $\alpha$  ( $\alpha = 2$  here). The upper-right grey region labelled ‘No Doppler Solutions’ is where  $A_{\text{obs}}$  is not possible, even for an edge-on binary. The lower-left blue region labelled ‘Weak Magnification’ is where the full range of allowed binary inclinations is at a higher latitude than required for significant lensing magnification.

restrict the binary inclination and mass ratio of the putative MBHB in PG 1302. We leave such an analysis for a future study.

Because measurements of  $n_a$ ,  $A_{\text{obs}}$ , and  $\alpha$  exist for the MBHB candidates plotted in Fig. 2, an analysis of the lensing probability under the assumption of a Doppler-boost origin could be readily examined for the known candidates. We leave this analysis, which should be accompanied by a more rigorous vetting of the Doppler assumption, for future work.

Note that this calculation, as well as the reverse calculation, the probability of observing the Doppler boost given a lensing flare, will depend on the relative brightness of the emitting regions around each BH and on the binary mass ratio. That is, the Doppler-boost signal should be present when a lensing signature is observed, but it can be diminished for near an equal-mass, circular binary where both components are moving at nearly opposite orbital speeds and are emitting at the same brightness.

### 3.3 Probe of binary orbit and accretion

In the point-source case, the observation of one or both lensing flares could exquisitely constrain the binary orbital inclination and mass ratio, two parameters which are otherwise difficult to constrain (e.g. D’Orazio et al. 2015b; Kun et al. 2015). As seen in Fig. 3, the magnification of either secondary or primary flare is very sensitive to the orbital inclination of the binary. Additionally, a measurement of the relative magnification of both flares would directly give the binary mass ratio (see Section 2.4). A non-detection of the second flare would put an upper limit on the binary mass ratio if the relative flux of each accretion disc structure can be determined from the primary flare.

As we have shown in Section 2.4, when the finite size of the lensed accretion disc becomes comparable to the *Einstein* radius of the lens, the lensing flare will have temporal structure that depends on the wavelength. Optical/IR radiation probes the cooler, outer regions of the disc, while shorter wavelength, UV to X-ray radiation probes the very inner regions of the disc where the point-source approximation is valid. Similar lensing tomography has been carried out to probe the accretion disc structure of multiply imaged quasars that suffer micro-lensing by stars in the lens galaxy (e.g. Kochanek et al. 2007; Dai et al. 2010; Jiménez-Vicente et al. 2015; Chartas et al. 2016). In the case of multiply imaged quasars, the source structure is probed by comparing changes in the flux ratios of multiple images due to an unknown distribution of stellar lenses. In contrast, the binary self-lensing technique has the advantage that the distance from source to lens, as well as the mass and trajectory of the lens, could be known with higher certainty. Also, self-lensing probes specifically the accretion discs around BHs in binaries, rather than the accretion discs around single BHs.

Observations of the lensing of both primary and secondary discs would allow us to separately study the contribution from both mini-discs. By elimination, the contribution from an outer circumbinary disc could also be identified. This would be invaluable to testing and informing theoretical work on the spectral signatures of circumbinary accretion discs (e.g. Generozov & Haiman 2014; Roedig et al. 2014; Farris et al. 2015), and circumbinary accretion in general.

If the source periodicity is overwhelmed by accretion disc variability rather than the Doppler boost, then the flare will not necessarily occur at the relative phase displayed in Figs 3, at the points of average brightness. However, a repeating flare on top of a periodic light curve that does not occur at the expected Doppler-boost phase will teach us when in the orbital phase accretion occurs on to the lensed BH, especially if a weaker Doppler-boost signal can be recovered for phase reference. This could allow us to test hydrodynamical models of accretion on to MBHBs, especially if multiple periods in the light curve are detected (e.g. D’Orazio et al. 2013, 2015a; Farris et al. 2014; Charisi et al. 2015).

If the Doppler variability is detected, the relative phase of the flare can be fixed and can act as an excellent tracer of binary orbital dynamics. If the discs surrounding the MBHBs are very massive, they could cause Newtonian precession of the orbit, or if the binary is compact enough (and eccentric), relativistic precession effects will become important. Orbital precession will cause the timing (pericentre precession) and magnitude (apsidal precession) of the flare to change, but the flare will always appear at the same relative phase in the light curve. Furthermore, the shape of the Doppler light curve will encode the orbital elements of the binary (e.g. only circular orbits considered here are sinusoidal). This scenario could allow high-precision measurements of precession effects.

Because the lensing flare reliably tracks the orbit of the binary and will be common for binaries near merger (see Fig. 2), the existence of a lensing flare would also facilitate attempts to track an EM chirp accompanying the GW chirp of a MBHB at merger<sup>2</sup> (Haiman 2017).

### 3.4 Extensions

Our calculations should apply to a wide range of real MBHBs. They do not, however, cover all possibilities. Below we list a set of

<sup>2</sup> Or a stellar mass BH+BH binary, or a BH+neutron star binary at merger if one of the binary components can emit bright EM emission (Schnittman et al. 2017).

possible extensions of this work that may apply to some MBHBs. These extensions would allow predictions which include lensing effects to be compared with observations of even more systems.

(i) We have not included the finite light travel time from the source accretion disc to the observer at different phases of the orbit. This will contribute an  $\mathcal{O}(v_{||}/c)$  effect to the Doppler plus lensing light curves, where  $v_{||}$  is the line-of-sight orbital velocity of the source.

(ii) Accretion disc variability (both stochastic and periodic components) could cause the flare magnitude to vary from orbit to orbit, but this can be tracked from the continuum light curve. Future work should also consider the amplitude of stochastic AGN variability relative to expected lensing magnification.

(iii) When considering finite-sized source effects we have not included the strong-field lensing of the source accretion disc by the source BH, which will alter the shape of the source for nearly edge-on accretion disc inclinations.

(iv) We have assumed that the binary is on a circular orbit throughout. If significant eccentricity exists in the orbit, the time-scale for the lensing flare will depend on the argument of pericentre.

(v) We have not fully considered the much more short-lived regime where the BHs are within 10s of Schwarzschild radii of each other and relativistic ray tracing must be performed rather than the point-mass lens approximation we make here. Future work should consider this case: while the residence time of the binary is short in this regime, the fraction of inclination angles for which strong-field lensing occurs approaches unity as the binary orbital separation approaches two Schwarzschild radii. If gas can follow close to merger, this lensing would be an almost necessary component of the electromagnetic counterparts to the GW sources of space-based gravitational wave detectors (LISA/PTAs) (see Haiman 2017). Such calculations are important for future all-sky surveys (e.g. the Large Synoptic Survey Telescope; Ivezić et al. 2008) and the Zwicky Transient Facility (Smith et al. 2014), which will monitor a larger number of AGN allowing the possibility of detecting even these rarest, compact MBHBs.

(vi) If the lensing BH has an optically thick accretion flow around it, with extent greater than its *Einstein* radius, the lensing flare would be blocked, but in this case we would expect an eclipse in place of the lensing flare with time-scale indicative of the primary disc size. If there is lensing of the primary accretion disc in the same system, eclipsing by and lensing of the primary accretion disc could provide independent constraints on the accretion disc size and opacity.

(vii) It is not clear whether or not a circumbinary disc will be aligned with the orbital plane of the binary (e.g. Miller & Krolik 2013; Aly et al. 2015). If the binary orbit is co-planar with a circumbinary disc, lensing flares could be obscured entirely. However, likely so would any other periodic emission from the binary mini-discs or circumbinary disc inner edge. In this case, the system would simply not be identified as a MBHB candidate via periodicity. It may be possible, however, to detect such periodically changing flux in the time-dependent broad line emission.

(viii) If there is a correlation between the binary angular momentum axis and the inclination of a surrounding dust torus, then it may be that the largest separation binaries, for which the binary inclination must be closest to edge on for significant lensing to occur, will be preferentially obscured. A lack of lensing events in confirmed MBHB candidates could even hint towards this scenario in the future. However, this would mean that closer to face-on systems could exhibit lensing flares in the IR, due to dust reverberation (e.g.

D’Orazio & Haiman 2017), such lensing echoes are the subject of future work.

## ACKNOWLEDGEMENTS

The authors thank Alberto Sesana, Maria Charisi, James Guillochon, Zoltán Haiman, Atish Kamble, Bence Kocsis, Avi Loeb, Frits Paerels, and Roman Rafikov for useful comments and discussions. The authors thank the anonymous referee for comments that improved the clarity of this manuscript. Financial support was provided from NASA through Einstein Postdoctoral Fellowship award number PF6-170151 (DJD) and also through the Smithsonian Institution and the Sprague Foundation (RD).

## REFERENCES

- Aly H., Dehnen W., Nixon C., King A., 2015, *MNRAS*, 449, 65  
 Armitage P. J., Natarajan P., 2005, *ApJ*, 634, 921  
 Barnes J. E., 2002, *MNRAS*, 333, 481  
 Barnes J. E., Hernquist L., 1992, *ARA&A*, 30, 705  
 Barnes J. E., Hernquist L., 1996, *ApJ*, 471, 115  
 Begelman M. C., Blandford R. D., Rees M. J., 1980, *Nature*, 287, 307  
 Bozza V., Capozziello S., Iovane G., Scarpetta G., 2001, *General Relativ. Gravitation*, 33, 1535  
 Charisi M., Bartos I., Haiman Z., Price-Whelan A. M., Márka S., 2015, *MNRAS*, 454, L21  
 Charisi M., Bartos I., Haiman Z., Price-Whelan A. M., Graham M. J., Bellm E. C., Laher R. R., Márka S., 2016, *MNRAS*, 463, 2145  
 Chartas G. et al., 2016, *Astron. Nachr.*, 337, 356  
 Cuadra J., Armitage P. J., Alexander R. D., Begelman M. C., 2009, *MNRAS*, 393, 1423  
 Dai X., Kochanek C. S., Chartas G., Kozłowski S., Morgan C. W., Garmire G., Agol E., 2010, *ApJ*, 709, 278  
 D’Orazio D. J., Haiman Z., 2017, *MNRAS*, 470, 1198  
 D’Orazio D. J., Haiman Z., MacFadyen A., 2013, *MNRAS*, 436, 2997  
 D’Orazio D. J., Haiman Z., Duffell P., Farris B. D., MacFadyen A. I., 2015a, *MNRAS*, 452, 2540  
 D’Orazio D. J., Haiman Z., Schiminovich D., 2015b, *Nature*, 525, 351  
 D’Orazio D. J., Haiman Z., Duffell P., MacFadyen A., Farris B., 2016, *MNRAS*, 459, 2379  
 Djorgovski S. G. et al., 2011, preprint (arXiv:1102.5004)  
 Dorn-Wallenstein T., Levesque E. M., Ruan J. J., 2017, *ApJ*, 850, 86  
 Drake A. J. et al., 2009, *ApJ*, 696, 870  
 Dunhill A. C., Cuadra J., Dougados C., 2015, *MNRAS*, 448, 3545  
 Farris B. D., Duffell P., MacFadyen A. I., Haiman Z., 2014, *ApJ*, 783, 134  
 Farris B. D., Duffell P., MacFadyen A. I., Haiman Z., 2015, *MNRAS*, 446, L36  
 Ferrarese L., Ford H., 2005, *Space Sci. Rev.*, 116, 523  
 Generozov A., Haiman Z., 2014, *MNRAS*, 443, L64  
 Gold R., Paschalidis V., Etienne Z. B., Shapiro S. L., Pfeiffer H. P., 2014a, *Phys. Rev. D*, 89, 064060  
 Gold R., Paschalidis V., Ruiz M., Shapiro S. L., Etienne Z. B., Pfeiffer H. P., 2014b, *Phys. Rev. D*, 90, 104030  
 Goodman J., 2003, *MNRAS*, 339, 937  
 Graham M. J. et al., 2015a, *MNRAS*, 453, 1562  
 Graham M. J. et al., 2015b, *Nature*, 518, 74  
 Haiman Z., 2017, *Phys. Rev. D*, 96, 023004  
 Haiman Z., Kocsis B., Menou K., 2009, *ApJ*, 700, 1952  
 Hayasaki K., Mineshige S., Sudou H., 2007, *Publ. Astron. Soc. Japan*, 59, 427  
 Jiménez-Vicente J., Mediavilla E., Kochanek C. S., Muñoz J. A., 2015, *ApJ*, 806, 251  
 Jun H. D., Stern D., Graham M. J., Djorgovski S. G., Mainzer A., Cutri R. M., Drake A. J., Mahabal A. A., 2015, *ApJ*, 814, L12  
 Kauffmann G., Haehnelt M., 2000, *MNRAS*, 311, 576

- Kochanek C. S., Dai X., Morgan C., Morgan N., Poindexter G. S. C., 2007, in Babu G. J., Feigelson E. D., eds, ASP Conf Ser. Vol. 371, Statistical Challenges in Modern Astronomy IV. Astron. Soc. Pac., San Francisco, p. 43
- Kormendy J., Ho L. C., 2013, ARA&A, 51, 511
- Kormendy J., Richstone D., 1995, ARA&A, 33, 581
- Kun E., Frey S., Gabányi K. É., Britzen S., Cseh D., Gergely L. Á., 2015, MNRAS, 454, 1290
- Lehto H. J., Valtonen M. J., 1996, ApJ, 460, 207
- Li Y.-R. et al., 2016, ApJ, 822, 4
- Li Y.-R. et al., 2017, preprint ([arXiv:1705.07781](https://arxiv.org/abs/1705.07781))
- Liu T. et al., 2015, ApJ, 803, L16
- Ivezic Z. et al., 2008, preprint ([arXiv:0805.2366](https://arxiv.org/abs/0805.2366))
- MacFadyen A. I., Milosavljević M., 2008, ApJ, 672, 83
- Mahabal A. A. et al., 2011, Bull. Astron. Soc. India, 39, 387
- Mayer L., 2013, Class. Quantum Gravity, 30, 244008
- Meiron Y., Kocsis B., Loeb A., 2017, ApJ, 834, 200
- Miller M. C., Krolik J. H., 2013, ApJ, 774, 43
- Milosavljević M., Merritt D., 2003, AIP Conf. Ser. Vol. 686, The Astrophysics of Gravitational Wave Sources. p. 201
- Muñoz D. J., Lai D., 2016, ApJ, 827, 43
- Noble S. C. et al., 2012, ApJ, 755, 51
- Paczynski B., 1986, ApJ, 304, 1
- Paczynski B., Rudak B., 1980, Acta Astron., 30, 237
- Papaloizou J., Pringle J. E., 1977, MNRAS, 181, 441
- Pursimo T. et al., 2000, A&AS, 146, 141
- Rahvar S., Mehrabi A., Dominik M., 2011, MNRAS, 410, 912
- Remillard R. A., McClintock J. E., 2006, ARA&A, 44, 49
- Roedig C., Sesana A., Dotti M., Cuadra J., Amaro-Seoane P., Haardt F., 2012, A&A, 545, A127
- Roedig C., Krolik J. H., Miller M. C., 2014, ApJ, 785, 115
- Schnittman J. D., Dal Canton T., Camp J., Tsang D., Kelly B. J., 2017, preprint ([arXiv:1704.07886](https://arxiv.org/abs/1704.07886))
- Sesana A., Haiman Z., Kocsis B., Kelley L. Z., 2017, preprint ([arXiv:1703.10611](https://arxiv.org/abs/1703.10611))
- Shapiro I. I., 1964, Phys. Rev. Lett., 13, 789
- Shi J.-M., Krolik J. H., 2015, ApJ, 807, 131
- Shi J.-M., Krolik J. H., Lubow S. H., Hawley J. F., 2012, ApJ, 749, 118
- Smith R. M. et al., 2014, in Proc. SPIE Vol. 9147, Ground-based and Airborne Instrumentation for Astronomy V. SPIE, Bellingham, p. 914779
- Zheng Z.-Y., Butler N. R., Shen Y., Jiang L., Wang J.-X., Chen X., Cuadra J., 2016, ApJ, 827, 56

This paper has been typeset from a  $\text{\LaTeX}$  file prepared by the author.